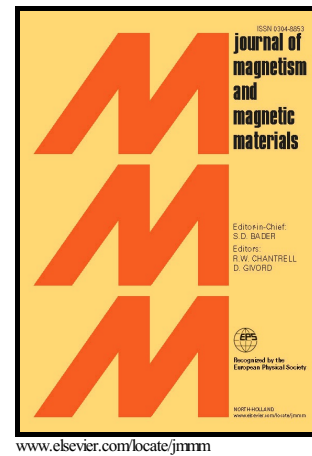


# Author's Accepted Manuscript

Structure and magnetic properties of ZnO coated MnZn ferrite nanoparticles

Shanigaram Mallesh, Annrose Sunny, Mutta Vasundhara, Veeturi. Srinivas



PII: S0304-8853(16)30214-1  
DOI: <http://dx.doi.org/10.1016/j.jmmm.2016.03.017>  
Reference: MAGMA61243

To appear in: *Journal of Magnetism and Magnetic Materials*

Received date: 30 November 2015  
Revised date: 4 March 2016  
Accepted date: 4 March 2016

Cite this article as: Shanigaram Mallesh, Annrose Sunny, Mutta Vasundhara and Veeturi. Srinivas, Structure and magnetic properties of ZnO coated MnZn ferrite nanoparticles, *Journal of Magnetism and Magnetic Materials* <http://dx.doi.org/10.1016/j.jmmm.2016.03.017>

This is a PDF file of an unedited manuscript that has been accepted for publication. As a service to our customers we are providing this early version of the manuscript. The manuscript will undergo copyediting, typesetting, and review of the resulting galley proof before it is published in its final citable form. Please note that during the production process errors may be discovered which could affect the content, and all legal disclaimers that apply to the journal pertain.

**Structure and magnetic properties of ZnO coated MnZn ferrite nanoparticles**Shanigaram Mallesh<sup>a</sup>, Annrose Sunny<sup>b</sup>, Mutta Vasundhara<sup>b</sup> and Veeturi Srinivas<sup>a\*</sup><sup>a</sup>*Department of Physics, Indian Institute of Technology Madras, Chennai-600036, India*<sup>b</sup>*Materials Science and Technology Division, CSIR-NIIST, Thiruvananthapuram, Kerala, 695019, India*

\*Corresponding author, Email; veeturi@iitm.ac.in

**Abstract**

A comparative study of structural and magnetic properties of MnZn ferrite (SF) and ZnO coated MnZn ferrite (ZF) nanoparticles (NPs) has been carried out. The as-prepared NPs show a single phase cubic spinel structure, with lattice parameter  $\sim 8.432$  Å. However  $\alpha$ -Fe<sub>2</sub>O<sub>3</sub> impurity phase emerge from SF particles when subjected to annealing at 600 °C in air. The weight fraction of  $\alpha$ -Fe<sub>2</sub>O<sub>3</sub> phase increases with increasing Mn concentration (9% for  $x=0.2$  and 53% for  $x=0.6$ ). On the other hand in ZF ( $x=0.2$  and 0.4) NPs no trace of impurity phase is observed when annealed at 600 °C. The magnetic measurements as a function of field and temperature revealed superparamagnetic like behavior with cluster moment  $\sim 10^4$   $\mu_B$  in as-prepared particles. The cluster size obtained from the magnetic data corroborates well with that estimated from structural analysis. Present results on ZnO coated MnZn ferrite particles suggest that an interfacial (ZnO@SF) reaction takes place during annealing, which results in formation of Zn-rich ferrite phase in the interface region. This leads to deterioration of magnetic properties even in the absence of  $\alpha$ -Fe<sub>2</sub>O<sub>3</sub> impurity phase.

**KEYWORDS:** Soft-ferrite, nanoparticles, magnetization, superparamagnet, microstructure.

## 1. Introduction

MnZn-ferrites are the important class of soft magnetic materials with wide range of technological applications due to their high initial permeability and low magnetic loss at higher frequencies. Ferrite nanoparticles (NPs) have been used in magnetic hyperthermia, ferrofluids, sensor technology, magnetic resonance imaging, biomedical and electromagnetic device applications [1-5]. It is well known that the magnetic properties of Mn-Zn ferrites depend on the sintering protocol, which directly affects the microstructure. Recently heat treatment effects on phase formation, microstructure and magnetic properties have been reported on  $Mn_xZn_{1-x}Fe_2O_4$  ( $x=0.5, 0.6$ ) ferrite NPs [5, 6]. Although these studies showed single phase (spinel structure) formation when as-prepared NPs are heat treated at 1200 °C [7, 8], impurity phases ( $\alpha-Fe_2O_3$ ) appear from NPs at moderate temperatures (600 °C-900 °C) [7-10]. This results in deterioration of soft magnetic properties of Mn-Zn ferrite fine particles. On the other hand heat treatment at moderate temperatures inhibits the grain growth and preserves low dimensional character of the material. Therefore the fine particles have to be processed in controlled conditions to avoid impurity phases and grain growth. One possible way to prevent the impurity phases is to encapsulate the particles with inert materials. This also helps in reducing the agglomeration of particles and restricts the grain growth [10]. For example chemically and thermally stable semiconducting oxides may be helpful as capping layer in two ways (i) restrict the direct interaction with atmosphere during annealing (ii) ferrimagnetic, semiconductor interfaces can bring changes in wide range of physical properties [11]. We have attempted to coat  $Mn_{0.6}Zn_{0.4}Fe_2O_4$  NPs with different nonmagnetic materials. These experiments showed that the ZnO coated particles are more effective in restricting the impurity phase compared to the other coatings [12]. The ZnO coating on

$\text{Mn}_{0.6}\text{Zn}_{0.4}\text{Fe}_2\text{O}_4$  NPs is useful on two counts: (i) it is biocompatible and stable oxide (ii) as being an important wide band-gap II–IV semiconductor and the ZnO layer around the ferrite NPs may be suitable for magneto-optic, spintronic devices as well as biomedical applications [11, 12]. The magnetic and electrical transport studies also indicate that Ferrite/ZnO bi-layer is more stable and has sharper interface compared to other bi-layers. Studies on these magnetic films at ambient temperature also suggest that despite somewhat reduced structural quality,  $\text{Fe}_3\text{O}_4$  on ZnO may prove to be a promising candidate for spin injection schemes [13]. Wang et al., suggested that  $\text{ZnFe}_2\text{O}_4$ –ZnO composite hollow microspheres can be useful for gas sensing, photocatalysis and magnetic resonance imaging [14].

In this paper we have synthesized MnZn spinel ferrite (SF) NPs through sol-gel process and coated with ZnO (ZF). These particles were annealed at 600 °C in air to obtain a core-shell structure NPs. Subsequently, structural and magnetic properties of as-prepared and annealed SF and ZF NPs have been investigated.

## 2. Experimental details

The MnZn spinel ferrite NPs were prepared by sol-gel method [8]. The composites of  $[(\text{Mn}_x\text{Zn}_{1-x}\text{Fe}_2\text{O}_4)_{(1-y)}(\text{ZnO})_y]$  ( $x=0.2, 0.4$  &  $0.6$ ;  $y=0, 0.3$ ) were synthesized through ultrasonication process as shown in Fig. 1. As-prepared NPs were dispersed in aqueous solution of  $\text{Zn}(\text{CH}_3\text{COO})_2 \cdot 2\text{H}_2\text{O}$  and then NaOH solution was added drop wise to this solution to maintain the pH at 8.0. Subsequently, the solution was ultrasonicated for one hour to break the agglomerated particles and to encapsulate ZnO on the surface of each particle. The slurry was washed several times with de-ionized water and dried at 70 °C. All the as-

prepared powder samples were annealed at 600 °C in air to investigate the microstructure and magnetic properties.

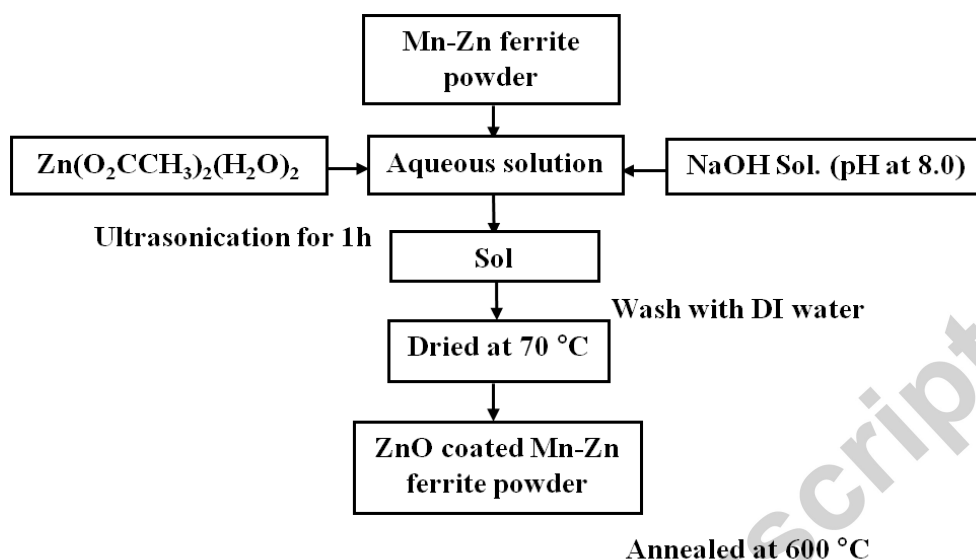


Fig. 1 The flow chart for the synthesis of ZnO coated MnZn ferrite NPs.

Structure and thermal stability of the samples was analyzed using X-ray diffraction (XRD) and thermal analysis. The XRD data was taken at RT (PANalytical X'pert PRO) from 20-80° (0.016 step in 2θ) with CuKα ( $\lambda=1.54059\text{\AA}$ ) radiation. The Raman spectra were recorded at 300 K with 633 nm emission line wavelength of He-Ne laser on a Jobin-Yvon LabRAM HR800UV spectrometer. Morphology, size distribution of the particles was analyzed with Transmission Electron Microscopy (TEM) TECNAI-30 G<sub>2</sub> S-Twin. Magnetic measurements were carried out using Quantum design Dynacool Physical property measurement system (ppms).

### 3. Results and discussions

Figure 2 shows the Rietveld refinement of XRD patterns of as-prepared and 600 °C air annealed SF, ZF samples. The presence of ZnO along with ferrite

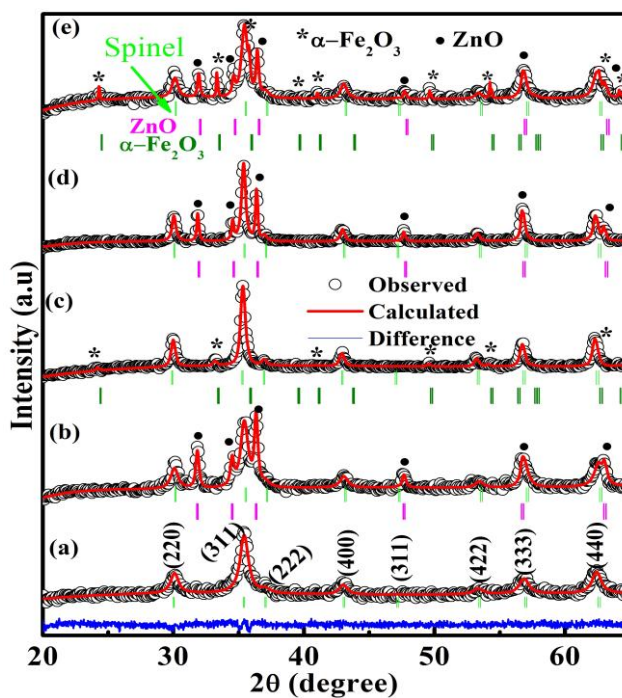


Fig. 2 Rietveld refinement of XRD patterns of (a) SF-as-prepared, (b) ZF-as-prepared (c) SF-600 °C (d) ZF-600 °C air annealed samples for  $x=0.2$  and (e) ZF-600 °C air annealed sample for  $x=0.6$ .

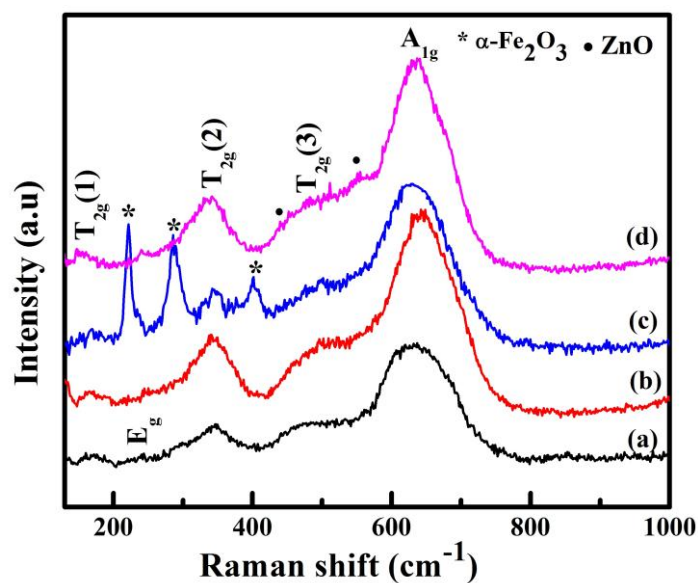
phase is detected in ZF as-prepared sample (Fig.2b). This observation suggests the existence of two phase structure and it can be viewed as ZnO shell with ferrite core. A secondary phase ( $\alpha\text{-Fe}_2\text{O}_3$ ), appeared in XRD pattern along with spinel phase (Fig. 2c), when as-prepared SF sample was annealed at 600 °C in air for 4h (see Table. I). On the other hand,  $\alpha\text{-Fe}_2\text{O}_3$  phase is absent for ZF sample and ZnO reflections along with SF spinel phase can be seen in Fig. 2d. Interestingly no impurity phase is observed in 600 °C annealed Zn-ferrite, but as the Mn concentration is increased fraction of  $\alpha\text{-Fe}_2\text{O}_3$  phase is increased. This observation suggests

that the presence of Mn in SF gives rise to impurity phases on annealing at 600 °C. Therefore, MnZn ferrite NPs with varying Mn concentration ( $x=0.2-0.6$ ) were prepared with optimum coating of ZnO to restrict the evolution of impurity phase. The results obtained from the refinement of XRD data are summarized in Table I. The 600 °C air annealed ZF samples exhibited a ferrite phase along with ZnO (without impurity  $\alpha\text{-Fe}_2\text{O}_3$ ) up to  $x=0.4$  concentration. However, small weight fraction of  $\alpha\text{-Fe}_2\text{O}_3$  phase appeared in  $\text{Mn}_{0.6}\text{Zn}_{0.4}\text{Fe}_2\text{O}_4\cdot(\text{ZnO})$  composition (Fig. 2e). These observations suggest that thicker coating of ZnO layer is necessary for higher Mn-containing ferrites to prevent the impure/secondary phases.

Table. I The structural parameters obtained from Rietveld refinement for SF, ZF as-prepared and 600 °C air annealed samples.  $T_a$ ,  $t$  and  $\chi^2$  represent annealing temperature, crystallite size and goodness of the fit respectively.

Samples		Lattice constants						wt (%)			
$T_a$	$t$ ( $\pm 1$ nm)	Spinel			ZnO			Spinel	$\alpha\text{-Fe}_2\text{O}_3$	ZnO	$\chi^2$
		a ( $\text{\AA}$ )	a=b ( $\text{\AA}$ )	c ( $\text{\AA}$ )	a=b ( $\text{\AA}$ )	c ( $\text{\AA}$ )					
SF ( $x=0.2$ )	As-prepared	14	8.4322 (7)	-	-	-	-	100	-	-	1.08
ZF ( $x=0.2$ )	As-prepared	9	8.4343 (8)	-	-	3.2519 (3)	5.2093 (4)	86.3(8)	-	13.7(8)	1.1
SF ( $x=0.2$ )	600°C	23	8.4369 (6)	5.0327 (2)	13.764 (8)	-	-	90.4(6)	9.5(6)	-	1.30
ZF ( $x=0.2$ )	600°C	23	8.4384 (4)	-	-	3.2512 (2)	5.2078 (3)	89.4(5)	-	10.5(5)	1.02
SF ( $x=0.4$ )	600°C	25	8.4366 (6)	5.0376 (4)	13.748 (2)	-	-	82.4(7)	17.6(7)	-	1.52
ZF ( $x=0.4$ )	600°C	21	8.4349 (6)	-	-	3.2508 (3)	5.2075 (5)	90.3(5)	-	9.7(5)	1.06
SF ( $x=0.6$ )	600°C	20	8.4431 (5)	5.0388 (3)	13.744 (6)	-	-	46.1(4)	53.8(4)	-	1.28
ZF ( $x=0.6$ )	600°C	15	8.4367 (7)	5.0384 (5)	13.747 (2)	3.2511 (3)	5.2074 (7)	82.0(3)	11.8(2)	6.0(2)	1.03

As shown in Table I the fraction of spinel phase increased due to the presence of ZnO shell in 600 °C annealed samples compared to that of as-prepared samples. The decrease of ZnO phase is almost same for  $x=0.2, 0.4$  concentrations. The average crystallite size ( $t$ ) is calculated by employing Scherrer's formula. The crystallite sizes of ZF as-prepared (9-13



nm) and annealed (15-23 nm) samples show lower than that of SF samples (see Table I), indicating that ZnO shell inhibits the grain growth during annealing. From the structural analysis it is further confirmed that ZnO is uniformly coated on the surface of SF NPs. These observations also indicate a possibility that a fraction of ZnO phase might be reacting with secondary  $\alpha\text{-Fe}_2\text{O}_3$  phase during the heat treatment to form Zn-rich ferrite phase. Similar results were reported in earlier work and suggested that the ZnO shell protects the SF from decomposition [10]. The ferrite phase successfully refined to the cubic spinel structure with  $Fd\text{-}3m$  space group (JCPDS file No.10-0467), ZnO to the hexagonal crystal structure with

63mc space group (JCPDS file No. 36-1451), while  $\alpha$ -Fe<sub>2</sub>O<sub>3</sub> to rhombohedral crystal structure with R-3c space group (JCPDS file No. 33-0664).

Fig. 3 Raman spectra of (a) SF-as-prepared, (b) ZF-as-prepared and (c) SF-600 °C, (d) ZF-600 °C air annealed samples for x=0.2 respectively.

The Raman spectra were recorded at 300 K in the frequency range from 100-1000 cm<sup>-1</sup>. According to the group theory five Raman active ( $A_{1g}+E_g+3T_{2g}$ ) modes were predicted for ferrites which belong to cubic spinel structure of AB<sub>2</sub>O<sub>4</sub> with Fd-3m space group [14]. In ferrites the Raman modes were assigned based on the relative motion of oxygen ions respect to tetrahedral (A) site ions in FeO<sub>4</sub>. The  $A_{1g}$  mode is due to symmetric stretch, of oxygen ions in FeO<sub>4</sub>,  $E_g$  and  $T_{2g}(3)$  modes are due to the symmetric and asymmetric bending of oxygen ions with respect to the Fe,  $T_{2g}(2)$  is symmetric stretch, of Fe and O and  $T_{2g}(1)$  is the translator motion of FeO<sub>4</sub> as total [15]. Fig. 3 shows the Raman spectra of as-prepared and 600 °C air annealed samples respectively. The as-prepared (Fig.3a) SF, (Fig.3b) ZF NPs exhibit ferrite Raman active modes, but  $E_g$  and  $T_{2g}(1)$  modes in low frequency region is not prominent which might be due to line broadening and strain on the surface of NPs. The  $\alpha$ -Fe<sub>2</sub>O<sub>3</sub> modes were detected in a SF sample annealed at 600 °C in air as shown in (Fig.3c). On the other hand pure ferrite modes were observed for ZF sample annealed at 600 °C (Fig.3d). These results corroborate well with XRD data. The ferrite modes observed  $A_{1g}$  (630- 640 cm<sup>-1</sup>)  $3T_{2g}$  (460- 500, 340-350, 154-170 cm<sup>-1</sup>) and  $E_g$  (150-175 cm<sup>-1</sup>) respectively. The modes of  $\alpha$ -Fe<sub>2</sub>O<sub>3</sub>  $A_{1g}$ ,  $E_g(2)$  and  $E_g(4)$  were observed at 220 cm<sup>-1</sup>, 283 cm<sup>-1</sup> and 401 cm<sup>-1</sup> respectively. The expected ZnO modes shown in Fig. 3 (d) are not discernible due to broadening of ferrite modes and superposition of peaks of ZnO with ferrite. Further we have observed (not shown here)  $A_1$  (2LO) mode around 1100 cm<sup>-1</sup> which is a finger print of ZnO [16].

High resolution transmission electron microscopy images of the as-prepared and 600 °C annealed ZF ( $x=0.2$ ) sample are shown in the Fig. 4. The TEM images show (Fig. 4(a), (b)) spherical shape particles with a marginal increase in particle size of annealed sample compared to that of as-prepared particles. The histograms shown in insets of Fig. 4(a), (b), suggest a narrow particle size distribution from 8-15 nm for as-prepared ZF NPs and 15-30 nm for annealed ZF sample. The size distribution of NPs was obtained by recording micrographs at different locations of the same sample and followed Gaussian distribution for

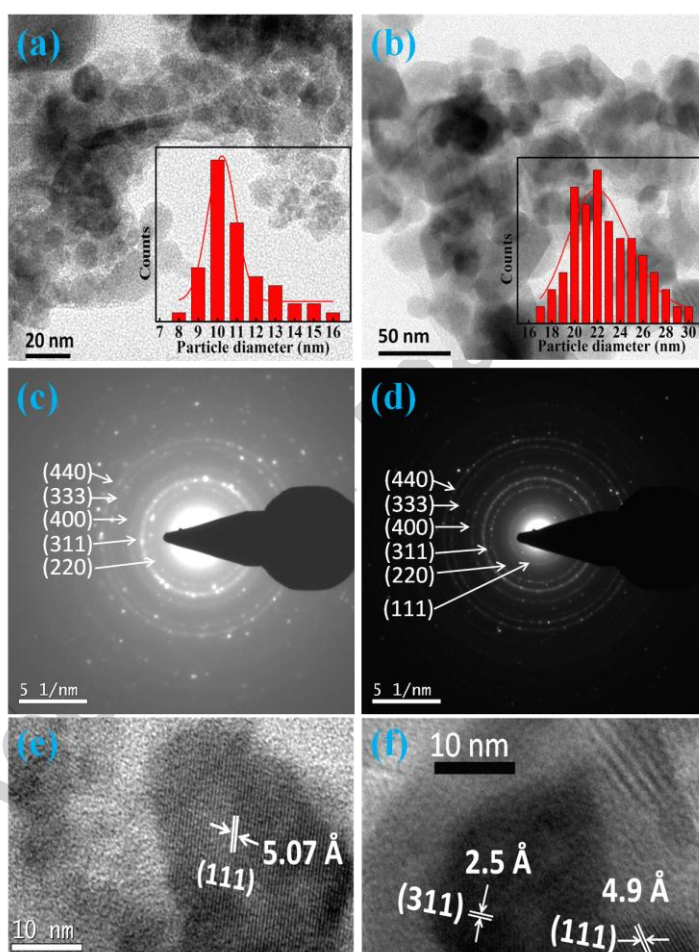
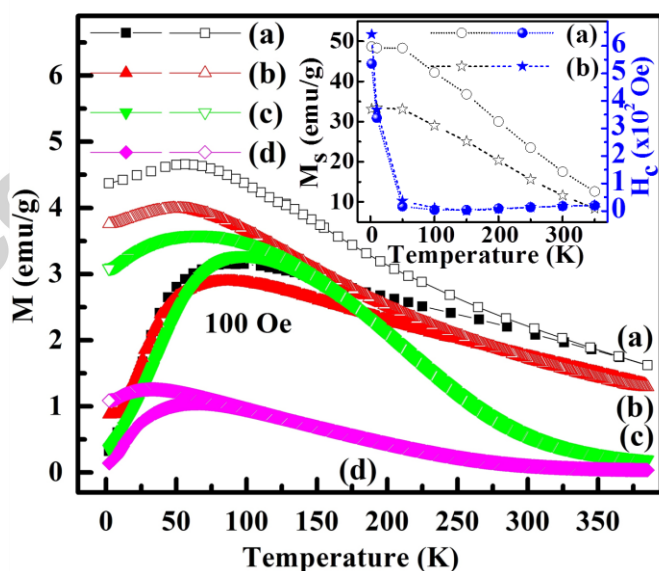


Fig. 4 (a, b) TEM images, (c, d) SAD patterns and (e, f) HR TEM of images of as-prepared and 600 °C air annealed ZF samples respectively.

ZF as-prepared and long-normal distribution for ZF 600 °C annealed samples. The selected area electron diffraction (SAD) pattern of as-prepared and annealed samples exhibit concentric rings indicating polycrystalline nature of samples (see Fig. 4(c), (d)). The lattice fringes correspond to a group of atomic planes within the NPs with distance between the two adjacent planes is  $\sim 5.07 \text{ \AA}$  for as-prepared,  $4.9 \text{ \AA}$  annealed samples and it is indexed to the (111) plane of spinel ferrites and  $2.5 \text{ \AA}$  is corresponding to the (311) plane of the ferrites. They exhibit single crystalline nature in limited area of the NP surface.

Figure 5 depicts the temperature (2-400K) variation of dc magnetization measured under magnetic field of 100 Oe following zero-field-cooled (ZFC) and field-cooled (FC) protocols. The observed ZFC magnetization exhibits a broad maximum at characteristic temperature ( $T_B$ ) below the FC-ZFC bifurcation temperature. Negligible coercivity ( $H_C$ ) and remanent



magnetization observed at  $T > T_B$  that suggests magnetic cluster blocking phenomenon. The broadening in ZFC maximum can be understood based on the relation  $KV = 25K_B T_B$ , where  $K$  is uniaxial anisotropy constant and  $V$  is the volume of the magnetic particles. Since the magnetic NPs have distribution of particle sizes ( $V$ ) (as observed from the TEM micrographs) a broad peak in ZFC magnetization curve is observed indicating a range of blocking temperatures. As shown in Fig. 5(a), (c) the  $T_B$  is estimated as  $\sim 95$  K, 100 K for as-prepared and annealed SF samples, while  $T_B$  is 85 K for as-prepared ZF which decreases to 65 K in the case of annealed ZF sample shown in Fig. 5(b), (d). The FC and ZFC curves exhibit similar behavior with a shift in maximum value. This shift of FC maximum (to lower temperatures) can be attributed to the alignment of larger particles in small applied fields [17]. The observed results are consistent with earlier reports on similar compositions. FC and ZFC curves exhibit irreversibility which appears near 305 K, 230 K for SF, ZF as-prepared samples and 120K, 85K for SF, ZF 600 °C annealed samples respectively. The FC magnetization is considered as equilibrium magnetization in the whole temperature range and ZFC magnetization as nonequilibrium measurement below the bifurcation temperature the spin relaxation time of the NPs very much greater than the measurement time (typically assumed to be  $\sim 10^3$  s for dc magnetization measurements) so the spins are frozen in random directions and the magnetization drops to smaller values [18]. In order to study the origin of magnetic disorder at low temperature, we have measured magnetization as a function of applied field at several temperatures below and above the  $T_B$ . The coercivity ( $H_c$ ) and saturation magnetization ( $M_s$ ) values are plotted as a function of temperature for as-prepared (a) SF and (b) ZF samples as shown inset of Fig. 5. The  $H_c$  drops by two orders of magnitude from 642 Oe at 2 K to 0.4 Oe at 100 K and remains constant upto 350 K. The  $M_s$  is

48.7emu/g at 2 K and decreases monotonously to 13 emu/g at 350 K for as-prepared SF sample. Similar behavior is observed in the case of as-prepared ZF sample. These observations support superparamagnetic (SPM) behavior. Earlier reports on MnZn ferrite NPs showed that the SPM limit is in the range of 20 nm [19]. Structural data (XRD and TEM) on presently studies of the samples show that the grain (particle) size is below SPM limit. The M-H curves measured at 2K and 300K (not shown here) for as-prepared and annealed NPs exhibit ferrimagnetic behavior at 2K and typical SPM at 300K. The SPM state in a material can be verified by plotting magnetization as a function of  $H/T$  ( $T > T_B$ ). The normalized isotherms above the  $T_B$  are plotted against  $H/T$  for SF and ZF as-prepared samples and found to superpose in certain range but small deviations are observed in the higher field region. The deviation from ideal SPM behavior might be due to the surface defects and presence of inter-particle interactions [17]. Further in order to identify the existence of single domain behavior below blocking temperature, the temperature dependence of  $H_C$  has been analyzed in the following. For a monodispersed and non-interacting single domain magnetic nanoparticles the temperature dependence of  $H_C$  is expressed as [20]

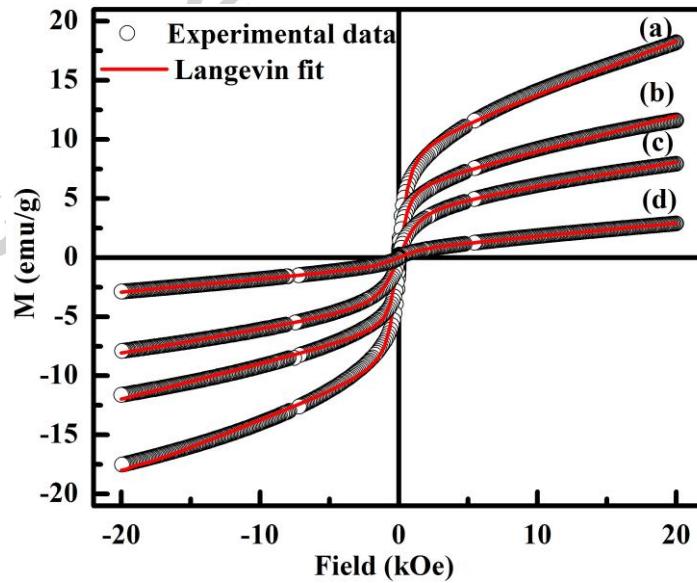
Fig. 5 The ZFC (filled )-FC (open ) magnetization measured at 100 Oe, (a) SF-as-prepared, (b) ZF-as-prepared and (c) SF-600 °C, (d) ZF-600 °C annealed samples for  $x=0.2$ . Inset, shows variation of  $M_s$  and  $H_c$  as a function of temperature for as-prepared SF and ZF samples respectively.

$$H_C(T) = H_C(0) \left[ 1 - \left( \frac{T}{T_B} \right)^{1/2} \right] \quad (1)$$

Where  $H_C(0)$  is the coercive field at  $T=0K$ , the  $H_C$  follow linear with  $T^{1/2}$  for non-interacting particles. The non-linear behavior of  $H_C$  with  $T^{1/2}$  is observed at high temperature for the as-prepared SF, ZF samples which indicate that the presence of interparticle interactions [17, 21]. The M-H curves of an SPM system is expected to follow the Langevin function. As shown in Fig. 6 magnetization data of as-prepared and annealed NPs has been fitted to a modified Langevin function equation [22]

$$M = M_s \left[ \coth\left(\frac{\mu H}{K_B T}\right) - \left(\frac{K_B T}{\mu H}\right) \right] + \chi H \quad (2)$$

where  $M_s$  is saturation magnetization,  $\mu$  is the magnetic moment of single particle,  $K_B$  is Boltzmann constant and  $\chi$  is the high field susceptibility. The deviation from ideal SPM is corrected with paramagnetic linear term and  $\chi$  is  $4.4 \times 10^{-4}$  emu/g.Oe,  $2.9 \times 10^{-4}$  emu/g.Oe for SF, ZF as-prepared samples and  $\chi$  is  $1.9 \times 10^{-4}$  emu/g.Oe,  $1.1 \times 10^{-4}$  emu/g.Oe for SF, ZF annealed samples. The particle moment is estimated from equation 2, which turns out to be



16390  $\mu_B$ , 17600  $\mu_B$  for SF, ZF as-prepared samples, while a decrease of an order of magnitude in moment is observed for annealed samples i.e, 8083  $\mu_B$ , 6654  $\mu_B$  for SF, ZF. The  $\mu$  values are very large which is an indication of each particle is composed with large number of spins. The average particle size can be estimated by using the expression  $\mu=d^3M_s/6$  where  $d$  is the diameter of particle assuming spherical shape. The average particle sizes are 10.8 ( $\pm 0.1$ ) nm, 10.5 ( $\pm 0.1$ ) nm for as-prepared SF, ZF NPs and 12 ( $\pm 0.1$ ) nm, 13 ( $\pm 0.1$ ) nm for annealed SF, ZF samples. These particle size values obtained from the fit for as-prepared samples are in good agreement with XRD TEM results, while deviation for annealed samples might be due decrease in effective magnetic particle size. The saturation magnetization values obtained from Langevin fit are smaller compared to the experimentally observed values. This difference can be attributed to the surface spins in the particles. A detailed analysis of magnetic data shows that both as-prepared and annealed ZF samples exhibit lower magnetization values compared to SF samples. The decrease in magnetic properties in ZF as-prepared sample might due to the presence of non-magnetic ZnO along with SF phase. Although it is concluded from the structural data of 600 °C annealed ZF sample that ZnO shell protects the SF from decomposition, the ZnO fraction is slightly decreases in stabilizing the ferrite phase. Further it is noticed that the magnetic properties deteriorate, which suggests the interfacial (ZnO@SF) reaction takes place during annealing and that may result in formation of Zn-rich ferrite phase. Further studies are in progress to verify the interfacial reaction and phase formation.

Fig. 6 Modified Langevin fit to the M-H curves measured at 300K for (a) SF-as-prepared, (b) ZF-as-prepared and (c) SF-600 °C, (d) ZF-600 °C air annealed samples for  $x=0.2$ .

#### 4. Conclusions

The ZnO coated MnZn (ZF) ferrite nanoparticles were synthesized and the physical properties are compared with uncoated NPs. The structural data reveals that the ZF NPs can be viewed in core (ferrite)-shell(ZnO) geometry. It has been shown that the evolution of  $\alpha$ -Fe<sub>2</sub>O<sub>3</sub> impurity phase in 600 °C annealed MnZn ferrite samples depend on Mn content. It is also demonstrated that impurity phase can be restricted by encapsulation of ZnO layers. The analysis of temperature and field dependence of magnetization data of the particles suggests SPM like behavior above a characteristic temperature. The particle size estimated from magnetization data corroborates well with the one obtained from structural data. The structure and magnetization studies indicate that there occurs an interfacial (ZnO@SF) reaction during annealing, which leads to the formation of Zn-rich ferrite phase in the interface region.

#### Acknowledgment

Dr. Vasundhara is thankful to CSIR, Govt. Of India, for the support regarding the characterization techniques received from sponsored project CSC0132.

#### References

- [1] V. Tsakaloudi, V. Zaspalis, *J. Magn. Magn. Mater.* 400 (2016) 307.
- [2] V. M. Khot, A. B. Salunkhe, J. M. Ruso, S. H. Pawar, *J. Magn. Magn. Mater.* 384 (2015) 335.
- [3] H. Yoon, J. S. Lee, J. H. Min, J. Wu, Y. K. Kim, *Nanoscale. Res. Lett.* 8 (2013) 530.
- [4] S. Dasgupta, J. Das, J. Eckert, and I. Manna, *J. Magn. Magn. Mater.* 306 (2006) 9.
- [5]. M. Zahraei, A. Monshi, M-P Morales, D. S. Gahrouei, M. Amirnasr, B. Behdadfar, *J. Magn. Magn. Mater.* 393 (2015) 429.
- [6] P. P. Naik, R. B. Tangsali, S. S. Meena, P. Bhatt, B. Sonaye, S. Sugur, *Rad. Phys. Chem.* 102 (2014) 147.

- [7] P. Hu, H. Yang, D. Pan, H. Wang, J. Tian, S. Zhang, X. Wang, A. Volinsky, *J. Magn. Magn. Mater.* 322 (2010) 173.
- [8] S. Mallesh, S. Kavita, R. Gopalan, V. Srinivas, *IEEE Trans. Magn.* 50 (2014) 2008204.
- [9] A. Angermann, J. Topfer, K. L. da Silva, K. D. Becker, *J. Alloys Compd.* 508 (2010) 433.
- [10] S. Mukherjee, K. Mukhopadhyay, S. Sutradhar, S. Pati, A. K. Deb, D. Das, P. K. Chakrabarti, *J. Phys. Chem. C.* 177 (2013) 12787.
- [11] S. Aydemir, S. Karakaya, *J. Magn. Magn. Mater.* 373 (2014) 33.
- [12] S. Mallesh, V. Srinivas, *AIP Conf. Proc.* 1665 (2015) 130039.
- [13] M. Paul, D. Kufer, A. Müller, S. Brück, E. Goering, M. Kamp, J. Verbeeck, H. Tian, G. Van Tendeloo, N. J. C. Ingle, M. Sing, and R. Claessen, *Appl. Phys. Lett.* 98 (2011) 012512.
- [14] S. Wang, X. Gao, J. Yang, Z. Zhu, H. Zhang, Y. Wang, *RSC Adv.* 4 (2014) 57967.
- [15] J. L. Verble, *Phys. Rev. B.* 9 (1974) 5236.
- [16] R. Cusco, E. A. Llado, J. Ibanez, L. Artus, J. Jimenez, B. Wang, M. J. Callahan, *Phys. Rev. B.* 75 (2007) 165202.
- [17] A. K. Pramanik, A. Banerjee, *Phys. Rev. B.* 82 (2010) 094402.
- [18] P. P. Vaishnava, U. Senaratne, E. C. Buc, R. Naik, V. M. Naik, G. M. Tsoi, L. E. Wenger, *Phys. Rev. B.* 76 (2007) 024413.
- [19] K. Mandal, S. Chakraverty, S. P. Mandal, P. Agudo, M. Pal, D. Chakravorty, *J. Appl. Phys.* 92 (2002) 501.
- [20] B. D. Cullity, *Introduction to Magnetic Materials* (Addison- Wesley, Philippines, 1972), Chap. 11.
- [21] B. Antic, M. Perovic, A. Kremenovic, J. Blanus, V. Spasojevic, P. Vulic, L. Bessais, E. S. Bozin, *J. Phys. Condens. Matter.* 25 (2013) 086001.
- [22] M. Tadic, S. Kralj, M. Jagodic, D. Hanzel, D. Makovec, *Appl. Surf. Sci.* 322 (2014) 255.

**Highlights**

- ✓ The properties of ZnO coated MnZn ferrite NPs are compared with uncoated NPs.
- ✓ The structural data reveals that the ZnO shell protects ferrite core from degradation.
- ✓ The field and temperature dependence of magnetization suggests SPM like behavior.
- ✓ From the magnetic isotherms average cluster moment is estimated to be  $\sim 10^4 \mu_B$ .
- ✓ Magnetic data suggests formation of Zn-rich ferrite phase in interfacial region.